JACS
JOURNAL OF THE AMERICAN CHEMICAL SOCIETY
pubs.acs.org/JACS
Article

Efficient Methane Electrosynthesis Enabled by Tuning Local CO_2 Availability

Xue Wang,[#] Aoni Xu,[#] Fengwang Li, Sung-Fu Hung, Dae-Hyun Nam, Christine M. Gabardo, Ziyun Wang, Yi Xu, Adnan Ozden, Armin Sedighian Rasouli, Alexander H. Ip, David Sinton, and Edward H. Sargent*

Cite This: https://dx.doi.org/10.1021/jacs.9b12445

ABSTRACT: The electroreduction of carbon dioxide (CO_2RR) to valuable chemicals is a promising avenue for the storage of intermittent renewable electricity. Renewable methane, obtained via CO_2RR using renewable electricity as energy input, has the potential to serve as a carbon-neutral fuel or chemical feedstock, and it is of particular interest in view of the well-established infrastructure for its storage, distribution, and utilization. However, CO_2RR to methane still suffers from low selectivity at commercially relevant current densities (>100 mA cm^{-2}). Density functional theory calculations herein reveal that lowering *CO_2 coverage on the Cu surface decreases the coverage of the *CO intermediate, and then this favors the protonation of *CO to *CHO, a key intermediate for methane generation, compared to the competing step, C−C coupling. We therefore pursue an experimental strategy wherein we control local CO_2 availability on a Cu catalyst by tuning the concentration of CO_2 in the gas stream and regulate the reaction rate through the current density. We achieve as a result a methane Faradaic efficiency (FE) of (48 ± 2)% with a partial current density of (108 ± 5) mA cm^{-2} and a methane cathodic energy efficiency of 20% using a dilute CO_2 gas stream. We report stable methane electrosynthesis for 22 h. These findings offer routes to produce methane with high FE and high conversion rate in CO_2RR and also make direct use of dilute CO_2 feedstocks.

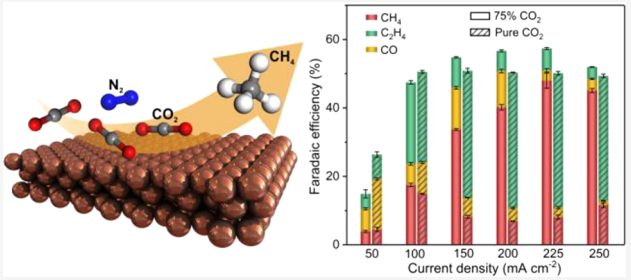

INTRODUCTION

The renewables-powered electroreduction of carbon dioxide (CO_2RR) is a promising strategy to convert CO_2 into carbon-neutral fuels and commodity chemicals.[1] A variety of products ranging from C_1 to C_3 have been reported in CO_2RR.[2−14] High Faradaic efficiency (FE) toward a single CO_2RR product at commercially relevant current densities (>100 mA cm^{-2}), however, has been reported only for carbon monoxide (CO) (FE ∼ 100%),[15,16] formate (FE > 80%),[17] and ethylene (70% FE).[18]

Methane, the simplest hydrocarbon product in CO_2RR and a widely used fuel,[2] is of particular interest, especially in light of the well-established infrastructure for natural gas storage, distribution, and consumption. Methane production from CO_2RR under conditions of ambient pressure and temperature represents a carbon-neutral alternative to fossil gas.[19]

To improve selectivity toward methane in CO_2RR, prior reports have focused on the tuning of Cu catalyst over morphology,[20−22] particle size,[23] and material structure.[24] Until now, the highest FE to methane, for systems operating with a total current density above 100 mA cm^{-2}, has been limited to a modest (18 ± 4)% (Table S1).[25−29] Techno-economic analyses show that commercial CO_2RR systems require operating current densities well above 100 mA cm^{-2} to be economically feasible.[16,30]

Here, we explore a new strategy to increase CO_2RR selectivity to methane at high current densities: we control local CO_2 availability at the catalyst surface. Density functional theory (DFT) calculations show that a reduction of *CO_2 coverage on the Cu surface favors the methane pathway compared to the competing C−C coupling pathway to C_2 products. Experimentally, we constrain *CO_2 coverage by tuning the concentration of CO_2 as well as by tuning reaction rates through the current density. We as a result achieve a methane FE of (48 ± 2)% with a partial current density >100 mA cm^{-2}.

RESULTS AND DISCUSSION

The catalyst for CO_2RR were prepared by sputtering a Cu layer (∼100 nm thick) on a polytetrafluoroethylene (PTFE) gas diffusion layer. As shown in the SEM image (Figure 1a),

Received: November 18, 2019
Published: January 28, 2020

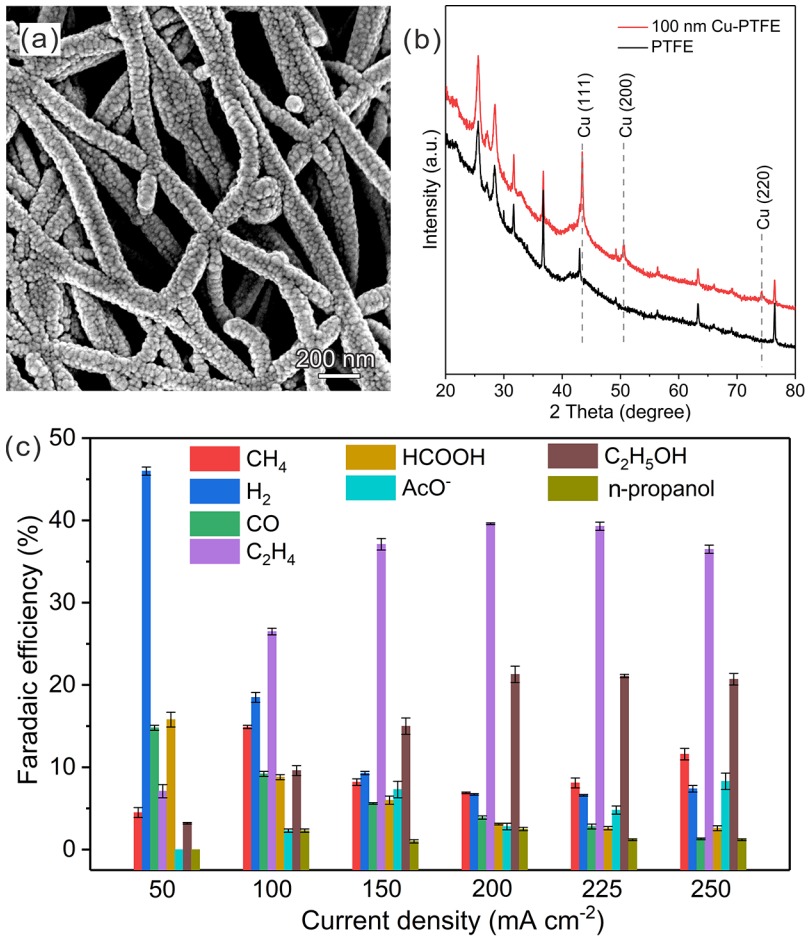

Figure 1. (a) Scanning electron microscopy (SEM) image of Cu on PTFE. (b) XRD patterns for Cu loaded on PTFE and the bare PTFE substrate. (c) Product FEs on Cu catalyst under different applied current densities in CO_2RR.

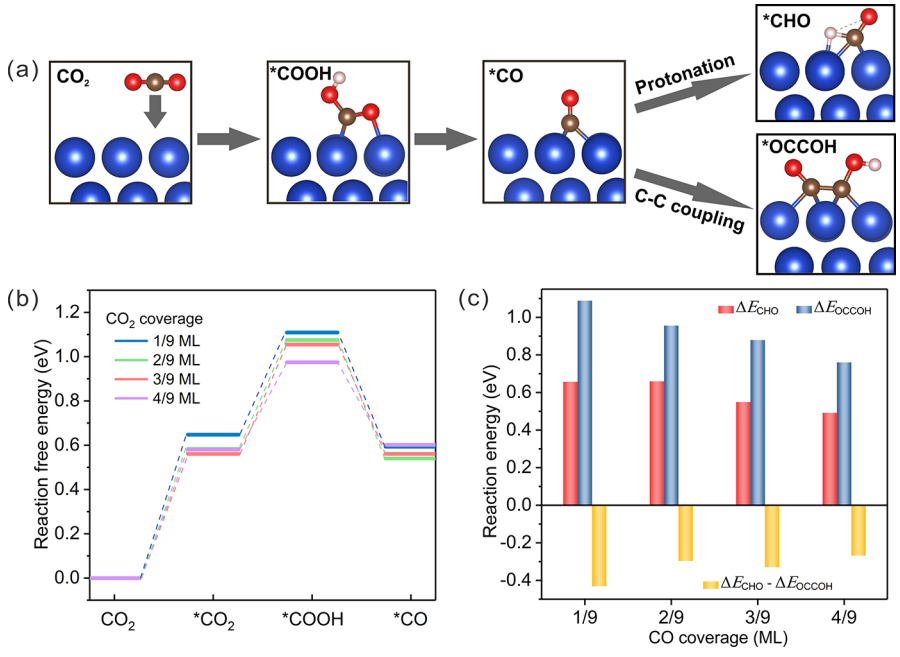

Figure 2. (a) Atomic models used in the calculations showing the pathways from CO_2 to *CO and then *CHO and *OCCOH. The catalyst active site was denoted by an asterisk (*). Red, brown, indigo, and pink balls stand for oxygen, carbon, copper, and hydrogen atoms, respectively. (b) Reaction free energies of CO_2 to *CO under different *CO_2 coverages. (c) Reaction energies of two competing reactions (protonation of *CO to *CHO, and C−C coupling) under different *CO coverages.

https://dx.doi.org/10.1021/jacs.9b12445
J. Am. Chem. Soc. XXXX, XXX, XXX−XXX

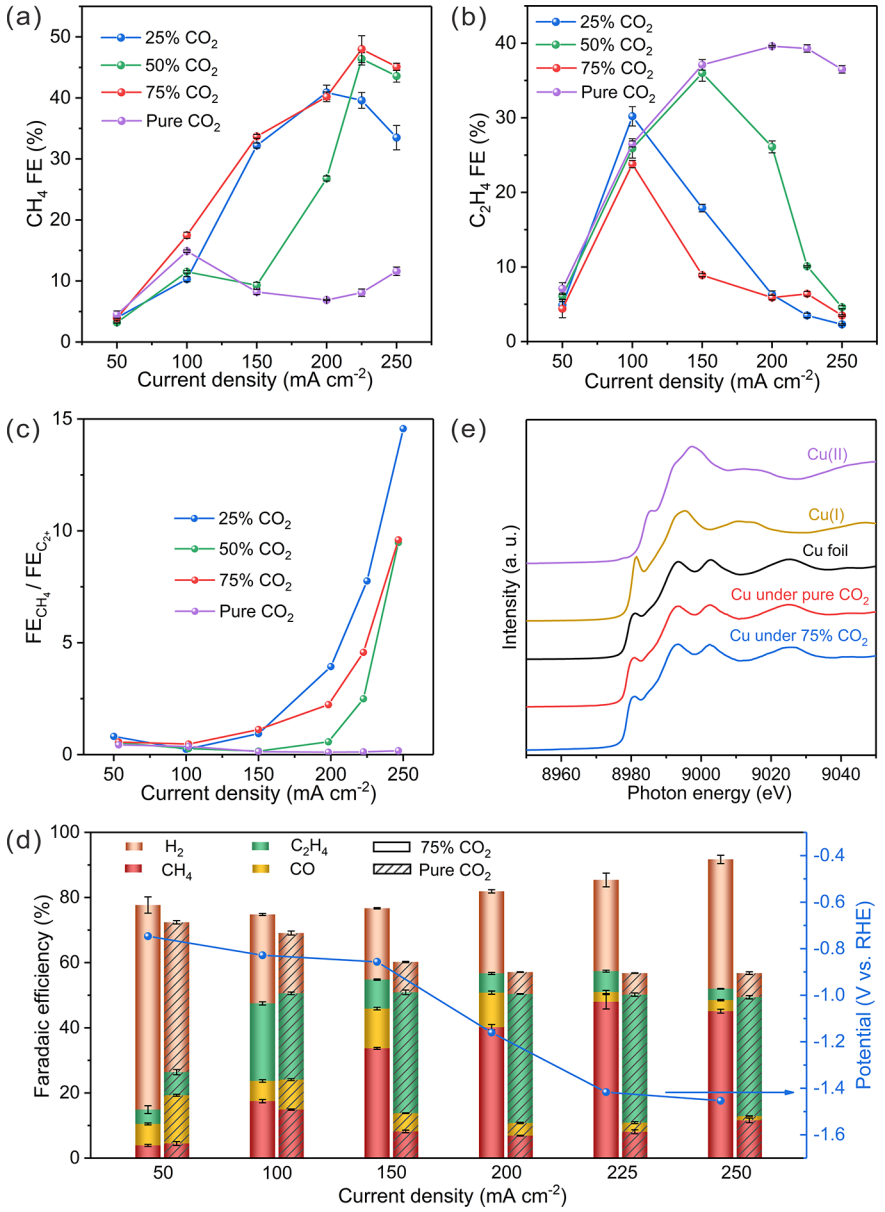

Figure 3. (a) Methane FEs and (b) ethylene FEs in CO_2RR at various CO_2 concentrations. (c) Comparison of the ratios of $FE_{methane}$ to FE_{C2+} on Cu catalysts at various CO_2 concentrations. (d) Gas product distribution under different applied current densities in CO_2RR using pure CO_2 and CO_2 concentration of 75%. (e) Operando Cu K-edge XANES spectra of Cu catalysts during CO_2RR at 200 mA cm^{-2} for 30 min using pure CO_2 and CO_2 concentration of 75% as the reactants, respectively. Bulk Cu foil, CuO, and Cu_2O are used as references.

the sputtered Cu layer on PTFE consists of many small nanoparticles. Powder X-ray diffraction (XRD) analysis of the catalyst confirms the existence of polycrystalline Cu (Figure 1b).

Using Cu catalyst as the working electrode, we conducted CO_2 electrolysis in a flow cell reactor[25] with a three-electrode configuration and CO_2-saturated 1 M $KHCO_3$ as the electrolyte. The results show that the maximum methane FE is 15% with partial methane current density of 15 mA cm^{-2} (Figure 1c), whereas C_2 products (ethylene and ethanol) are the main products.

We then sought to investigate, using DFT, the reason underlying the low selectivity to methane. Previous reports[31−34] have suggested the pathway from CO_2 to methane on a Cu surface is CO_2 → *COOH → *CO, followed by *CO → *CHO →⋯→ *CH_4. After *CO generation, the main step competing with *CO protonation is C−C coupling to C_2 products.[35,36] Prior studies focusing, for example, on ethylene production, show that local *CO coverage affects the product distribution in CO_2RR.[37,38] We investigated therefore the connection between the local CO_2 surface coverage and methane selectivity on Cu catalysts. We first calculated the reaction free energies of CO_2 to *CO intermediate. The reaction free energy of CO_2 to *COOH ($\Delta G_{*COOH\text{-}CO_2}$) is the effective barrier[39] for CO_2 to *CO (Figure 2a,b, Figure S1, and Table S2). We found that lowering the coverage of CO_2 on Cu surface increases $\Delta G_{*COOH\text{-}CO_2}$ and thus leads to a lower *CO coverage.

We further investigated the impact of the resulting difference in *CO coverage on the post-*CO pathways: *CO protonation to *CHO (a key reaction in methane pathway) vs C−C coupling for C_2 products.[34−36] We calculated the

https://dx.doi.org/10.1021/jacs.9b12445
J. Am. Chem. Soc. XXXX, XXX, XXX−XXX

reaction energies of *CO to *CHO (ΔE_{CHO}) and C−C coupling (ΔE_{OCCOH}) at different *CO coverage levels (Figure 2c and Figure S2).[37,38] We found that, with increasing *CO coverage from 1/9 to 4/9 monolayer (ML), both ΔE_{CHO} and ΔE_{OCCOH} decrease. However, using the value of ($\Delta E_{CHO} - \Delta E_{OCCOH}$) as the descriptor for the tendency to *CHO vs C−C coupling, we found that lower *CO coverage improves methane selectivity vs C_2 products.

Taken together, these DFT studies suggest that lowering *CO_2 coverage on the Cu surface promotes selectivity to methane in CO_2RR. We then explored experimental means to regulate CO_2 surface coverage by tuning local CO_2 concentration. We rationalized this strategy according to Henry's law: local CO_2 concentration is positively related with local CO_2 partial pressure; local CO_2 partial pressure is then proportional to the CO_2 surface coverage.[39,40]

We evaluated the CO_2RR performance at various CO_2 concentrations (25%, 50%, 75%, and 100%) by tuning the volume ratios of CO_2 to N_2 in the gas streams (Figure 3a,b, Figure S3, and Table S3). We found that, at low reaction rates (≤100 mA cm^{-2}), both methane FEs and ethylene FEs at various CO_2 concentrations were similar (Figure 3a,b); at high reaction rates (150−250 mA cm^{-2}), methane FEs in dilute CO_2 increased, while ethylene FEs decreased, relative to those in pure CO_2. The methane FEs start to decrease after the peak values in dilute CO_2 (Figure 3a), which we attribute to CO_2 mass transport limitation:[41] the produced *CO is not enough for the *CO protonation step for methane production and the pathways for C_{2+} products (Figure 3b and Table S3).

The influence of *CO_2 coverage on methane selectivity is further supported by plotting the ratio of methane FE to the total FE of C_{2+} products ($FE_{methane}/FE_{C2+}$) as a function of current density at various CO_2 concentrations (Figure 3c). In the region of high current density (200−250 mA cm^{-2}), $FE_{methane}/FE_{C2+}$ increases along with the decrease of CO_2 concentration, demonstrating that low CO_2 availability, induced by low concentration CO_2 and high current density, favors methane production, in agreement with calculations herein.

We observed that, while methane selectivity increased using diluted CO_2 streams, H_2 FEs were also higher than that at pure CO_2 (Figure S3a). The result suggests that the competing hydrogen evolution reaction (HER)[42] is promoted on the Cu surface at dilute CO_2, which is consistent with calculation results (Table S4). With dilute CO_2, the high concentration of adsorbed hydrogen atoms (H_{ad}) generated via the Volmer step ($H^+ + e^- \rightarrow H_{ad}$) in HER favors the protonation of the *CO intermediate to *CHO,[31,43] a factor that contributes to the improvement in selectivity for methane production.

Using dilute CO_2 streams, we achieved a new level of methane selectivity compared to prior reports at current densities >100 mA cm^{-2}. We compared the FEs for gas products at CO_2 concentration of 75% and pure CO_2 (Figure 3d). At 225 mA cm^{-2}, we achieved a methane FE of (48 ± 2)% with a partial current density of (108 ± 5) mA cm^{-2} at −1.416 V relative to the reversible hydrogen electrode (V_{RHE}) after ohmic loss correction. The corresponding methane cathodic energy efficiency is 20%. SEM results show no observable morphology difference between Cu catalysts (following CO_2RR) for CO_2 concentration of 75% vs pure CO_2 (Figure S4).

We acquired operando X-ray absorption spectra (XAS) at the Cu K-edge to investigate the Cu chemical state during CO_2RR (Figure 3e). The average valence states of copper under pure CO_2 and CO_2 concentration of 75% are zero: we conclude that product selectivity differences are not associated with any notable difference in the valence states of copper.[9,44]

We further studied the stability of CO_2RR at CO_2 concentration of 75% in CO_2-saturated 1 M $KHCO_3$ electrolyte (Figure 4). The current density was fixed at 225 mA cm^{-2} during the electrolysis process. The methane FE was steady at (48 ± 2)% with a high partial methane current density of (108 ± 5) mA cm^{-2} for more than 20 h and then decreased to 42% after 22 h. The corresponding potential was stable during the 22 h of operating time.

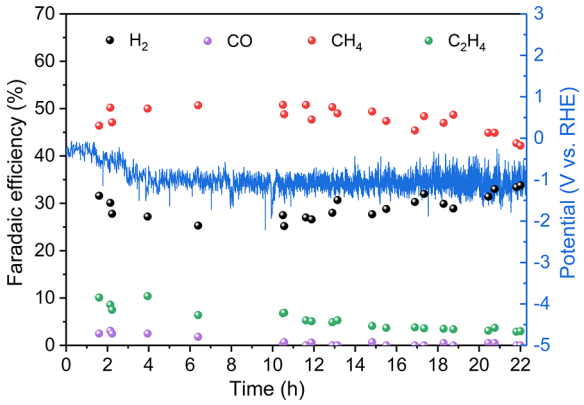

Figure 4. Performance test of CO_2RR to methane during 22 h of electrolysis under the current density of 225 mA cm^{-2} at CO_2 concentration of 75%.

CONCLUSIONS

This work demonstrates that the control of local CO_2 availability on Cu catalyst enables methane production with high efficiency in CO_2RR. Using DFT, we assess the reaction free energies of the *CO intermediate under different *CO_2 coverages as well as the reaction energies of the key steps branching methane versus C_2 products. The calculation results show that a lowering of the *CO_2 coverage on Cu could decrease *CO coverage and thus favor the protonation of *CO for methane production. We then tune local CO_2 availability on the Cu catalyst by controlling the CO_2 concentration in the feedstock and regulating the reaction rate through current density. We achieve a FE of (48 ± 2)% toward methane at a high methane conversion rate of (108 ± 5) mA cm^{-2} with a CO_2 concentration of 75%, together with a high methane cathodic energy efficiency of 20%. We further demonstrate that this CO_2RR system can operate for over 22 h by keeping methane FE over 42%.

This work provides a strategy to direct-convert dilute CO_2 feedstock to carbon-neutral methane with high selectivity and high conversion rate. Previous CO_2RR studies use pure CO_2 as the reactant stream;[2−18] however, CO_2 feedstocks with a range of concentrations are directly available in industrial processes such as petroleum refineries, coal power plant, cement production, and iron and steel manufacture.[45] The CO_2 purification of these streams can be simplified when dilute CO_2 streams are used as reactants directly for desired products with high FE and high current density in CO_2RR.

https://dx.doi.org/10.1021/jacs.9b12445
J. Am. Chem. Soc. XXXX, XXX, XXX−XXX

EXPERIMENTAL DETAILS

Electrode Preparation. Cu cathodes were prepared by sputtering the Cu catalyst with a layer thickness of 100 nm (Cu target, sputtering rate: ~1.1 Å s^{-1}) on a piece of PTFE membrane (an average pore size of 450 nm; Beijing Zhongxingweiye Instrument Co., Ltd.) by using a magnetron sputtering system. Ni foam with a thickness of 1.6 mm (MTI Corporation) and Ag/AgCl reference electrode (3 M KCl, BASi) were used as the anode and reference electrode, respectively.

Structure and Composition Characterizations. SEM images were taken using a Hitachi S-5200 microscope. Structural characterization of cathodes was obtained using XRD (MiniFlex600) with Cu Kα radiation. XAS measurements were conducted with the HXMA beamline at Canadian Light Source. Athena and Artemis software included in a standard IFEFFIT package were used to process XAS data.[46]

Electrochemical Measurements. All the electrochemical measurements were conducted in a three-electrode system in a flow cell using an electrochemical workstation (AUT50783). Prepared cathodes, anion exchange membrane (Fumasep FAB-PK-130), and nickel foam were positioned and clamped together via PTFE gaskets. Before the measurement, CO_2 gas (Linde, 99.99%) was purged in a 1 M $KHCO_3$ aqueous solution for 30 min. CO_2-saturated 1 M $KHCO_3$ aqueous solution (30 mL) was introduced into the cathode chamber and the anode chamber, respectively, using two pumps at the rate of 10 mL min^{-1}. During the whole electrochemical test, CO_2 was kept in a purging state in the catholyte. Pure CO_2 gas (Linde, 99.99%) or N_2-diluted CO_2 gas with CO_2 concentrations of 25%, 50%, and 75% was continuously supplied to the gas chamber of the flow cell at a flow rate of 90 mL min^{-1}. The CO_2RR performance was tested using constant-current electrolysis. All potentials vs Ag/AgCl reference electrode were converted to values vs RHE using the equation: $E_{RHE} = E_{Ag}/_{AgCl} + 0.210\ V + 0.0591 \times \text{pH}$. The electrochemical impedance spectroscopy (EIS) technique was used to evaluate the ohmic loss between the working and reference electrodes, and 80% *i*R compensation was applied to correct the potentials manually. Gas products were analyzed using a gas chromatograph (PerkinElmer Clarus 600) equipped with thermal conductivity and flame ionization detectors. Liquid products were analyzed by a nuclear magnetic resonance spectrometer (Agilent DD2 600 MHz), and dimethyl sulfoxide was used as an internal standard.

By assuming that the overpotential of oxygen evolution reaction on the anode side is zero, we calculated methane cathodic energy efficiency ($EE_{\text{cathodic half-cell}}$) as follows[18]

$$EE_{\text{cathodic half-cell}} = \frac{(1.23 + (-E_{methane})) \times FE_{methane}}{(1.23 + (-E_{applied}))}$$

where $E_{applied}$ is the potential used in the experiment,$FE_{methane}$ is the measured Faradaic efficiency of methane in percentage, and $E_{methane}$ = 0.17 V_{RHE} for CO_2RR.[47]

Theoretical methods. In this work, all DFT calculations were carried out with periodic slab models using the Vienna ab initio simulation program (VASP).[48−51] The generalized gradient approximation (GGA) was used with the Perdew−Burke−Ernzerhof (PBE) exchange-correlation functional.[52] The electron−ion interactions was described by the projector-augmented wave (PAW) method,[53,54] and the cutoff energy for the plane-wave basis set was 450 eV. In all calculations, the atoms at all positions have Hellmann−Feynman forces lower than 0.02 eV $Å^{-1}$, and the electronic iterations convergence was 10^{-5} eV using the Normal algorithm. A 4-layer (3 × 3) Cu(111) supercell was built to simulate the exposed surface of copper accompanied with a sufficient vacuum gap of 15 Å. Structural optimizations were performed on all modified slab models with a grid of (3 × 3 × 1) k-point.

Surface $*CO_2$ or *CO coverages were set to 1/9 to 4/9 ML (Figures S1 and S2). Here, 1/9 ML means one CO_2 or CO molecule on the Cu(111) surface of the p(3 × 3) super cell. The reaction free energies of CO_2 to *CO on catalyst surface at various $*CO_2$ coverages were simulated based on the following reactions

$$*CO_2 + H_2O + e^- \rightarrow *COOH + OH^-$$

$$*COOH + e^- \rightarrow *CO + OH^-$$

According to previous reported reaction pathways,[32−36] the product selectivity of CO_2 reduction is strongly dependent on two competing reactions starting from *CO intermediate: *CO protonation for CH_4 production and C−C coupling, respectively.

$$*CO \text{ protonation for } CH_4 \text{ prod: } *CO + H_2O + e^- \rightarrow *CHO + OH^-$$

$$\text{C−C coupling: } *CO + *CO + H_2O + e^- \rightarrow *OCCOH + OH^-$$

The reaction free energies (ΔG) were calculated using the expression $\Delta G = \Delta E - T\Delta S$, where ΔE is the reaction energy obtained by the difference between the reactant and product molecules absorbed on the catalyst surface, ΔS is the change in entropy for each reaction, and T is the absolute temperature (in Kelvin). Entropy values of gaseous molecules are taken from the standard database,[55] while the entropies of adsorbate and adsorption site are negligible. The reaction energies of *CO protonation and C−C coupling were calculated at 0 V_{RHE}.

ASSOCIATED CONTENT

Supporting Information

The Supporting Information is available free of charge at https://pubs.acs.org/doi/10.1021/jacs.9b12445.

Adsorption configurations of CO_2, *COOH, and *CO on Cu(111) surface with different $*CO_2$ coverages; adsorption configurations of *CO, *CHO, and *OCCO on Cu(111) surface with different *CO coverages; H_2, CO, and liquid product FEs on Cu catalysts in CO_2RR at various CO_2 concentrations; SEM images of Cu on PTFE following CO_2RR using CO_2 concentration of 75% and pure CO_2 as the reactants; performance comparison of CO_2-to-methane with total current density higher than 100 mA cm^{-2}; $\Delta G_{*\text{COOH-CO}_2}$ under different *CO coverages; reaction energies of Volmer step ($H^+ + e^- \rightarrow H_{ad}$) in HER under different *CO coverages. (PDF)

AUTHOR INFORMATION

Corresponding Author

Edward H. Sargent − *Department of Electrical and Computer Engineering, University of Toronto, Toronto, Ontario M5S 1A4, Canada;* orcid.org/0000-0003-0396-6495; Email: ted.sargent@utoronto.ca

Authors

Xue Wang − *Department of Electrical and Computer Engineering, University of Toronto, Toronto, Ontario M5S 1A4, Canada;* orcid.org/0000-0002-6298-1858

Aoni Xu − *Department of Electrical and Computer Engineering, University of Toronto, Toronto, Ontario M5S 1A4, Canada*

Fengwang Li − *Department of Electrical and Computer Engineering, University of Toronto, Toronto, Ontario M5S 1A4, Canada;* orcid.org/0000-0003-1531-2966

Sung-Fu Hung − *Department of Electrical and Computer Engineering, University of Toronto, Toronto, Ontario M5S 1A4, Canada*

Dae-Hyun Nam − *Department of Electrical and Computer Engineering, University of Toronto, Toronto, Ontario M5S 1A4, Canada;* orcid.org/0000-0002-0871-1355

Christine M. Gabardo − *Department of Mechanical and Industrial Engineering, University of Toronto, Toronto, Ontario M5S 3G8, Canada;* orcid.org/0000-0002-9456-6894

https://dx.doi.org/10.1021/jacs.9b12445
J. Am. Chem. Soc. XXXX, XXX, XXX−XXX

Ziyun Wang − *Department of Electrical and Computer Engineering, University of Toronto, Toronto, Ontario M5S 1A4, Canada;* orcid.org/0000-0002-2817-8367
Yi Xu − *Department of Mechanical and Industrial Engineering, University of Toronto, Toronto, Ontario M5S 3G8, Canada;* orcid.org/0000-0002-8108-0975
Adnan Ozden − *Department of Mechanical and Industrial Engineering, University of Toronto, Toronto, Ontario M5S 3G8, Canada*
Armin Sedighian Rasouli − *Department of Electrical and Computer Engineering, University of Toronto, Toronto, Ontario M5S 1A4, Canada*
Alexander H. Ip − *Department of Electrical and Computer Engineering, University of Toronto, Toronto, Ontario M5S 1A4, Canada*
David Sinton − *Department of Mechanical and Industrial Engineering, University of Toronto, Toronto, Ontario M5S 3G8, Canada;* orcid.org/0000-0003-2714-6408

Complete contact information is available at: https://pubs.acs.org/10.1021/jacs.9b12445

Author Contributions

#X.W. and A.X. contributed equally.

Notes

The authors declare no competing financial interest.

■ ACKNOWLEDGMENTS

This work was supported by Natural Gas Innovation Fund, the Natural Sciences and Engineering Research Council (NSERC) of Canada, and Natural Resources Canada Clean Growth Program, and Ontario Research Fund − Research Excellence program. All DFT computations were performed on the Niagara supercomputer at the SciNet HPC Consortium. SciNet is funded by the Canada Foundation for Innovation, the Government of Ontario, Ontario Research Fund Research Excellence Program, and the University of Toronto. All of the XAS research described in this paper was performed at the Canadian Light Source, a national research facility of the University of Saskatchewan, which is supported by the Canada Foundation for Innovation (CFI), the Natural Sciences and Engineering Research Council (NSERC), the National Research Council (NRC), the Canadian Institutes of Health Research (CIHR), the Government of Saskatchewan, and the University of Saskatchewan. The authors thank Chen, N. and Chen, W. for technical support at the 06ID-1(HXMA) beamline in CLS. D.S. acknowledges the NSERC E.W.R. Steacie Memorial Fellowship. C.M.G. acknowledges support from NSERC in the form of a postdoctoral fellowship.

■ REFERENCES

(1) Jhong, H.-R. M.; Ma, S.; Kenis, P. J. A. Electrochemical conversion of CO_2 to useful chemicals: current status, remaining challenges, and future opportunities. *Curr. Opin. Chem. Eng.* **2013**, *2*, 191.
(2) Hori, Y. Electrochemical CO_2 Reduction on Metal Electrodes. In *Modern Aspects of Electrochemistryno.42*; Vayenas, C. G., White, R. E., Gamboa-Aldeco, M. E., Eds.; Springer: New York, 2008; chap. 3.
(3) Qiao, J.; Liu, Y.; Hong, F.; Zhang, J. A review of catalysts for the electroreduction of carbon dioxide to produce low-carbon fuels. *Chem. Soc. Rev.* **2014**, *43*, 631.
(4) Benson, E. E.; Kubiak, C. P.; Sathrum, A. J.; Smieja, J. M. Electrocatalytic and homogeneous approaches to conversion of CO_2 to liquid fuels. *Chem. Soc. Rev.* **2009**, *38*, 89−99.
(5) Kim, D.; Kley, C. S.; Li, Y.; Yang, P. Copper nanoparticle ensembles for selective electroreduction of CO_2 to C_2−C_3 products. *Proc. Natl. Acad. Sci. U. S. A.* **2017**, *114*, 10560.
(6) Liu, Y.; Chen, S.; Quan, X.; Yu, H. Efficient electrochemical reduction of carbon dioxide to acetate on nitrogen-doped nanodiamond. *J. Am. Chem. Soc.* **2015**, *137*, 11631.
(7) Yang, D.; Zhu, Q.; Chen, C.; Liu, H.; Liu, Z.; Zhao, Z.; Zhang, X.; Liu, S.; Han, B. Selective electroreduction of carbon dioxide to methanol on copper selenide nanocatalysts. *Nat. Commun.* **2019**, *10*, 677.
(8) Mistry, H.; Varela, A. S.; Bonifacio, C. S.; Zegkinoglou, I.; Sinev, I.; Choi, Y.-W.; Kisslinger, K.; Stach, E. A.; Yang, J. C.; Strasser, P.; Cuenya, B. R. Highly selective plasma-activated copper catalysts for carbon dioxide reduction to ethylene. *Nat. Commun.* **2016**, *7*, 12123.
(9) Zhou, Y.; Che, F.; Liu, M.; Zou, C.; Liang, Z.; Luna, P. D.; Yuan, H.; Li, J.; Wang, Z.; Xie, H.; Li, H.; Chen, P.; Bladt, E.; Quintero-Bermudez, R.; Sham, T.-K.; Bals, S.; Hofkens, J.; Sinton, D.; Chen, G.; Sargent, E. H. Dopant-induced electron localization drives CO_2 reduction to C_2 hydrocarbons. *Nat. Chem.* **2018**, *19*, 974.
(10) Ren, D.; Ang, B. S.-H.; Yeo, B. S. Tuning the selectivity of carbon dioxide electroreduction toward ethanol on oxide-derived Cu_xZn catalysts. *ACS Catal.* **2016**, *6*, 8239.
(11) Rahaman, M.; Dutta, A.; Zanetti, A.; Broekmann, P. Electrochemical reduction of CO_2 into multicarbon alcohols on activated Cu mesh catalysts: an identical location (IL) study. *ACS Catal.* **2017**, *7*, 7946.
(12) De Luna, P.; Hahn, C.; Higgins, D.; Jaffer, S. A.; Jaramillo, T. F.; Sargent, E. H. What would it take for renewably powered electrosynthesis to displace petrochemical processes? *Science* **2019**, *350*, No. eaav3506.
(13) Liu, M.; Pang, Y.; Zhang, B.; Luna, P. D.; Voznyy, O.; Xu, J.; Zheng, X.; Dihn, C. T.; Fan, F.; Cao, C.; Pelayo Garcia de Arquer, F.; Safaei, T. S.; Mepham, M.; Klinkova, A.; Kumacheva, E.; Filleter, T.; Sinton, D.; Kelley, S. O.; Sargent, E. H. Enhanced electrocatalytic CO_2 reduction via field-induced reagent concentration. *Nature* **2016**, *537*, 382.
(14) Gao, S.; Lin, Y.; Jiao, X.; Sun, Y.; Luo, Q.; Zhang, W.; Li, D.; Yang, J.; Xie, Y. Partially oxidized atomic cobalt layers for carbon dioxide electroreduction to liquid fuel. *Nature* **2016**, *529*, 68−71.
(15) Ren, S.; Joulié, D.; Salvatore, D.; Torbensen, K.; Wang, M.; Robert, M.; Berlinguette, C. P. Molecular electrocatalysts can mediate fast, selective CO_2 reduction in a flow cell. *Science* **2019**, *365*, 367.
(16) Gabardo, C. M.; Seifitokaldani, A.; Edwards, J. P.; Dinh, C.-T.; Burdyny, T.; Kibria, M. G.; O'Brien, C. P.; Sargent, E. H.; Sinton, D. Combined high alkalinity and pressurization enable efficient CO_2 electroreduction to CO. *Energy Environ. Sci.* **2018**, *11*, 2531.
(17) Xia, C.; Zhu, P.; Jiang, Q.; Pan, Y.; Liang, W.; Stavitsk, E.; Alshareef, H. N.; Wang, H. Continuous production of pure liquid fuel solutions via electrocatalytic CO_2 reduction using solid-electrolyte devices. *Nat. Energy* **2019**, *4*, 776.
(18) Dinh, C.-T.; Burdyny, T.; Kibria, M. D.; Seifitokaldani, A.; Gabardo, C. M.; Pelayo Garcia de Arquer, F.; Kiani, A.; Edwards, J. P.; Luna, P. D.; Bushuyev, O. S.; Zou, C.; Quintero-Bermudez, R.; Pang, Y.; Sinton, D.; Sargent, E. H. CO_2 electroreduction to ethylene via hydroxide-mediated copper catalysis at an abrupt interface. *Science* **2018**, *360*, 783.
(19) Howarth, R. W.; Ingraffea, A. Should fracking stop? *Nature* **2011**, *477*, 271.
(20) Qiu, Y.-L.; Zhong, H.-X.; Zhang, T.-T.; Xu, W.-B.; Li, X.-F.; Zhang, H.-M. Copper electrode fabricated via pulse electrodeposition: toward high methane selectivity and activity for CO_2 electroreduction. *ACS Catal.* **2017**, *7*, 6302.
(21) Manthiram, K.; Beberwyck, B. J.; Alivisatos, A. P. Enhanced electrochemical methanation of carbon dioxide with a dispersible nanoscale copper catalyst. *J. Am. Chem. Soc.* **2014**, *136*, 13319.
(22) Li, Y.; Cui, F.; Ross, M. B.; Kim, D.; Sun, Y.; Yang, P. Structure-sensitive CO_2 electroreduction to hydrocarbons on ultrathin 5-fold twinned copper nanowires. *Nano Lett.* **2017**, *17*, 1312.

(23) Reske, R.; Mistry, H.; Behafarid, F.; Cuenya, B. R.; Strasser, P. Particle size effects in the catalytic electroreduction of CO_2 on Cu nanoparticles. *J. Am. Chem. Soc.* **2014**, *136*, 6978.
(24) Zhao, H.; Chang, X.; Chen, J. G.; Goddard III, W. A.; Xu, B.; Cheng, M.-J.; Lu, Q. Computational and experimental demonstrations of one-pot tandem catalysis for electrochemical carbon dioxide reduction to methane. *Nat. Commun.* **2019**, *10*, 3340.
(25) Zhuang, T.-T.; Pang, Y.; Liang, Z.-Q.; Wang, Z.; Li, Y.; Tan, C.-S.; Li, J.; Dinh, C. T.; Li, F.; Proppe, A.; Johnston, A.; Nam, D.-H.; Wu, Z.-Y.; Zheng, Y.-R.; Ip, A. H.; Tan, H.; Chen, L.-J.; Yu, S.-H.; Kelly, S. O.; Sinton, D.; Sargent, E. H. Copper nanocavities confine intermediates for efficient electrosynthesis of C3 alcohol fuels from carbon monoxide. *Nat. Catal.* **2018**, *1*, 946.
(26) Ma, S.; Sadakiyo, M.; Heima, M.; Luo, R.; Haasch, R. T.; Gold, J. I.; Yamauchi, M.; Kenis, P. J. A. Electroreduction of carbon dioxide to hydrocarbons using bimetallic Cu−Pd catalysts with different mixing patterns. *J. Am. Chem. Soc.* **2017**, *139*, 47.
(27) Jiang, K.; Sandberg, R. B.; Akey, A. J.; Liu, X.; Bell, D. C.; Nørskov, J. K.; Chan, K.; Wang, H. Metal ion cycling of Cu foil for selective C−C coupling in electrochemical CO_2 reduction. *Nat. Catal.* **2018**, *1*, 111.
(28) Hoang, T. T. H.; Verma, S.; Ma, S.; Fister, T. T.; Timoshenko, J.; Frenkel, A. I.; Kenis, P. J. A.; Gewirth, A. A. Nanoporous copper−silver alloys by additive-controlled electrodeposition for the selective electroreduction of CO_2 to ethylene and ethanol. *J. Am. Chem. Soc.* **2018**, *140*, 5791.
(29) Li, Y. C.; Wang, Z.; Yuan, T.; Nam, D.-H.; Luo, M.; Wicks, J.; Chen, B.; Li, J.; Li, F.; Pelayo Garcia de Arquer, F.; Wang, Y.; Dinh, C.-T.; Voznyy, O.; Sinton, D.; Sargent, E. H. Binding site diversity promotes CO_2 electroreduction to ethanol. *J. Am. Chem. Soc.* **2019**, *141*, 8584.
(30) Jouny, M.; Luc, W.; Jiao, F. General techno-economic analysis of CO_2 electrolysis systems. *Ind. Eng. Chem. Res.* **2018**, *57*, 2165.
(31) Peterson, A. A.; Nørskov, J. K. Activity descriptors for CO_2 electroreduction to methane on transition-metal catalysts. *J. Phys. Chem. Lett.* **2012**, *3*, 251.
(32) Kortlever, R.; Shen, J.; Schouten, K. J. P.; Calle-Vallejo, F.; Koper, M. T. Catalysts and reaction pathways for the electrochemical reduction of carbon dioxide. *J. Phys. Chem. Lett.* **2015**, *6*, 4073.
(33) Cheng, T.; Xiao, H.; Goddard III, W. A. Reaction mechanisms for the electrochemical reduction of CO_2 to CO and formate on the Cu(100) surface at 298 K from quantum mechanics free energy calculations with explicit water. *J. Am. Chem. Soc.* **2016**, *138*, 13802.
(34) Xiao, H.; Cheng, T.; Goddard III, W. A. Atomistic mechanisms underlying selectivities in C_1 and C_2 products from electrochemical reduction of CO on Cu(111). *J. Am. Chem. Soc.* **2017**, *139*, 130.
(35) Cheng, T.; Xiao, H.; Goddard, W. A. Full atomistic reaction mechanism with kinetics for CO reduction on Cu(100) from ab initio molecular dynamics free-energy calculations at 298 K. *Proc. Natl. Acad. Sci. U. S. A.* **2017**, *114*, 1795.
(36) Liu, X.; Schlexer, P.; Xiao, J.; Ji, Y.; Wang, L.; Sandberg, R. B.; Tang, M.; Brown, K. S.; Peng, H.; Ringe, S.; Hahn, C.; Jaramillo, T. F.; Nørskov, J. K.; Chan, K. pH effects on the electrochemical reduction of $CO_{(2)}$ towards C_2 products on stepped copper. *Nat. Commun.* **2019**, *10*, 32.
(37) Huang, Y.; Handoko, A. D.; Hirunsit, P.; Yeo, B. S. Electrochemical reduction of CO_2 using copper single-crystal surfaces: effects of CO* coverage on the Selective formation of ethylene. *ACS Catal.* **2017**, *7*, 1749.
(38) Li, J.; Wang, Z.; McCallum, C.; Xu, Y.; Li, F.; Wang, Y.; Gabardo, C. M.; Dinh, C.-T.; Zhuang, T.-T.; Wang, L.; Howe, J. Y.; Ren, Y.; Sargent, E. H.; Sinton, D. Constraining CO coverage on copper promotes high-efficiency ethylene electroproduction. *Nat. Catal.* **2019**, *2*, 1124.
(39) Wang, Z.; Cao, X. M.; Zhu, J.; Hu, P. Activity and coke formation of nickel and nickel carbide in dry reforming: a deactivation scheme from density functional theory. *J. Catal.* **2014**, *311*, 469.
(40) Wang, Z.; Wang, H.-F.; Hu, P. Possibility of designing catalysts beyond the traditional volcano curve: a theoretical framework for multi-phase surfaces. *Chem. Sci.* **2015**, *6*, 5703.
(41) Li, C. W.; Ciston, J.; Kanan, M. W. Electroreduction of carbon monoxide to liquid fuel on oxide-derived nanocrystalline copper. *Nature* **2014**, *508*, 504.
(42) Marković, N. M.; Ross, P. N. Surface science studies of model fuel cell electrocatalysts. *Surf. Sci. Rep.* **2002**, *45*, 117.
(43) Zhang, Y.-J.; Sethuraman, V.; Michalsky, R.; Peterson, A. A. Competition between CO_2 reduction and H_2 evolution on transition-metal electrocatalysts. *ACS Catal.* **2014**, *4*, 3742.
(44) Li, J.; Che, F.; Pang, Y.; Zou, C.; Howe, J. Y.; Burdyny, T.; Edwards, J. P.; Wang, Y.; Li, F.; Wang, Z.; Luna, P. D.; Dinh, C.-T.; Zhuang, T.-T.; Saidaminov, M. I.; Cheng, S.; Wu, T.; Finfrock, Y. Z.; Ma, L.; Hsieh, S.-H.; Liu, Y.-S.; Botton, G. A.; Pong, W.-F.; Du, X.; Guo, J.; Sham, T.-K.; Sargent, E. H.; Sinton, D. Copper adparticle enabled selective electrosynthesis of n-propanol. *Nat. Commun.* **2018**, *9*, 4614.
(45) Bains, P.; Psarras, P.; Wilcox, J. CO_2 capture from the industry sector. *Prog. Energy Combust. Sci.* **2017**, *63*, 146.
(46) Ravel, B.; Newville, M. ATHENA, ARTEMIS, HEPHAESTUS: data analysis for X-ray absorption spectroscopy using IFEFFIT. *J. Synchrotron Radiat.* **2005**, *12*, 537.
(47) Kuhl, K. P.; Cave, E. R.; Abram, D. N.; Jaramillo, T. F. New insights into the electrochemical reduction of carbon dioxide on metallic copper surfaces. *Energy Environ. Sci.* **2012**, *5*, 7050−7059.
(48) Kresse, G.; Hafner, J. *Ab initio* molecular dynamics for liquid metals. *Phys. Rev. B: Condens. Matter Mater. Phys.* **1993**, *47*, 558−561.
(49) Kresse, G.; Hafner, J. *Ab initio* molecular-dynamics simulation of the liquid-metal−amorphous-semiconductor transition in germanium. *Phys. Rev. B: Condens. Matter Mater. Phys.* **1994**, *49*, 14251.
(50) Kresse, G.; Furthmüller, J. Efficient iterative schemes for *ab initio* total-energy calculations using a plane-wave basis set. *Phys. Rev. B: Condens. Matter Mater. Phys.* **1996**, *54*, 11169.
(51) Kresse, G.; Furthmuller, J. Efficiency of ab-initio total energy calculations for metals and semiconductors using a plane-wave basis set. *Comput. Mater. Sci.* **1996**, *6*, 15.
(52) Perdew, J. P.; Burke, K.; Ernzerhof, M. Generalized gradient approximation made simple. *Phys. Rev. Lett.* **1996**, *77*, 3865.
(53) Blöchl, P. E. Projector augmented-wave method. *Phys. Rev. B: Condens. Matter Mater. Phys.* **1994**, *50*, 17953.
(54) Kresse, G.; Joubert, D. From ultrasoft pseudopotentials to the projector augmented-wave method. *Phys. Rev. B: Condens. Matter Mater. Phys.* **1999**, *59*, 1758.
(55) Chase, M. W. NIST-JANAF thermochemical tables for oxygen fluorides. *J. Phys. Chem. Ref. Data* **1996**, *25*, 551.

https://dx.doi.org/10.1021/jacs.9b12445
J. Am. Chem. Soc. XXXX, XXX, XXX−XXX